Structural and Double Layer Forces between Silica Surfaces in Suspensions of Negatively Charged Nanoparticles

Scarratt, Liam Ronald John; Kubiak-Schaaf, Katarzyna Joanna; Maroni, Plinio; Trefalt, Gregor; Borkovec, Michal

Published in Langmuir 2020, 36, 14443−14452

https://dx.doi.org/10.1021/acs.langmuir.0c02917

Structural and double layer forces between silica surfaces in suspensions of negatively charged nanoparticles

Liam R. J. Scarratt, Katarzyna Kubiak, Plinio Maroni, Gregor Trefalt, Michal Borkovec*

Department of Inorganic and Analytical Chemistry, University of Geneva, Sciences II, 30 Quai Ernest-Ansermet, 1205 Geneva, Switzerland

*Corresponding author: Email: michal.borkovec@unige.ch

Abstract

Direct force measurements between negatively charged silica microparticles are carried out in suspensions of like-charged nanoparticles with the atomic force microscope (AFM). In agreement with previous studies, oscillatory force profiles are observed at larger separation distances. At smaller distances, however, soft and strongly repulsive forces are present. These forces are caused by double layer repulsion between the like-charged surfaces and can be quantitatively interpreted with the Poisson-Boltzmann (PB) model. However, the PB model must be adapted to a strongly asymmetric electrolyte to capture the non-exponential nature of these forces. Thereby, the nanoparticles are modeled as highly charged co-ions, while the counter ions are monovalent. This model permits to extract the effective charge of the nanoparticles, which is well comparable to the one obtained from electrophoresis. The PB model also explains the presence of a particle-free layer close to the interface.

Introduction

Concentrated suspensions of charged nanoparticles are relevant in numerous applications, such as, papermaking, ceramic processing, or food technology.[1-5] Such systems come again into focus of fundamental research due to recent reports of structural forces acting between like-charged surfaces.[6-14] These forces are normally probed in suspensions of negatively charged silica nanoparticles sandwiched between two silica surfaces by means the colloidal probe atomic force microscopy (AFM).[15-17] One typically observes oscillatory profiles with a wavelength of several nanometers featuring several of these oscillations. The wavelength λ of these oscillations was suggested to be related to the number concentration c of the nanoparticles as[10,12]

$$\lambda = c^{-1/3} \tag{1}$$

This dependence originates from the double layer repulsion between the nanoparticles, which forces them into a liquid-like structure. Equation (1) follows from geometrical considerations by identifying the wavelength with the spacing between nearest neighbors in a close-packed structure. The same scaling dependence was observed with X-rays or neutrons, in particular, with small angle scattering through the position of the structural peak in bulk suspensions[12,18] or with reflectivity near an isolated interface.[19,20]

Similar oscillatory forces were also observed in concentrated polyelectrolyte[21-24] and micellar solutions.[25,26] While this similarity is not surprising for spherical micelles, an analogous structuring also occurs in polyelectrolyte solutions. In the latter case, the wavelength follows the scaling law given in eq. (1) only at lower concentrations. A similar scaling law remains applicable at higher concentrations, albeit with a different exponent.[23,27,28]

Less information is available on double layer forces acting in these systems. In the standard experiments the nanoparticles and the planar (or quasi-planar) surfaces are negatively charged. Therefore, the presence of strongly repulsive double layer forces is expected too. Additional exponential repulsive forces were found recently in such systems, but these forces seem relatively weak.[29] In solutions of polyelectrolytes, strongly repulsive double layer forces were recently reported by some of us.[28] In the latter case, these forces were non-exponential, but compatible with predictions of Poisson-Boltzmann (PB) theory.

Structuring and forces in colloidal suspensions of charged particles have also attracted much attention in the theoretical community.[30-33] Thereby, a more rigorous description beyond the PB theory was pursued, typically with computer simulations or integral equation theories. Some researchers have considered the so-called primitive model, where the macroions and counter ions are treated on equal footing. Another approach is to only treat the nanoparticles in an explicit fashion and consider the presence of counter ions by assuming that their mutual interaction is described by screened Coulomb potential. Fewer studies focused on structuring near planar interfaces or interactions of such surfaces.[34-37] One among the latter studies addressed interactions between charged interfaces where the co-ions were multivalent.[34] Structuring in suspensions of colloidal particles interacting with screened Coulomb potential was also investigated near hard and charged walls and within a slits.[38,37] These studies also report the formation of oscillatory force (or density) profiles, whereby the wavelength was also found to follow eq. (1).[18]

The present article addresses the question of double layer forces in charged nanoparticle suspensions between like-charged substrates from the experimental point of view. In these systems, we also show evidence of repulsive and non-exponential double layer forces acting at shorter distances. These forces can be interpreted with classical PB theory. Quantitative analysis leads to estimates of the effective charge of the nanoparticles in question.

Poisson-Boltzmann model

Consider an asymmetric 1:*Z* electrolyte solution containing monovalent cations of charge +1 and point-like multivalent ions of charge –*Z* that is sandwiched between two infinite, charged plates. The number concentration of the macroions in the bulk will be denoted as *c*, while the concentration of the monovalent ions is *Zc*. This system can be described with the Poisson-Boltzmann (PB) equation[1,16,39]

$$\frac{d^2\psi}{dx^2} = \frac{qc}{\varepsilon_0\varepsilon}\left(e^{\beta qZ\psi} - Ze^{-\beta q\psi}\right) \tag{2}$$

where q is the elementary charge, ε_0 the permittivity of vacuum, ε the dielectric constant of water, and $\beta = 1/(kT)$ whereby T is the absolute temperature and k the Boltzmann constant. We use $\varepsilon = 80$ as appropriate for water at room temperature. Equation (2) is solved numerically between two identical plates positioned at $x = \pm h/2$ where h is the separation between the plates, subject to the boundary conditions[39]

$$\pm\varepsilon_0\varepsilon \left.\frac{d\psi}{dx}\right|_{x=\pm h/2} = \sigma - C_{\text{in}}[\psi(\pm h/2) - \psi_{\text{dl}}] \tag{3}$$

where σ and ψ_{dl} are the surface charge density and the diffuse layer potential of the isolated surface, and C_{in} its inner capacitance. This condition includes charge regulation effects within the constant regulation (CR) approximation. The former parameters are related with the charge-potential relationship. For the 1:Z electrolyte considered, this relationship reads

$$\sigma = \text{sgn}(\psi_{\text{dl}})\left[2kT\varepsilon_0\varepsilon c\left(Ze^{-\beta q\psi_{\text{dl}}} + e^{\beta qZ\psi_{\text{dl}}} - 1 - Z\right)\right]^{1/2} \quad (4)$$

where sgn() denotes the sign function. Instead of the inner capacitance, we consider the regulation parameter *p*, which is defined as[40]

$$p = \frac{C_{\text{dl}}}{C_{\text{in}} + C_{\text{dl}}} \quad (5)$$

where C_{dl} is the diffuse layer capacitance given by[39]

$$C_{\text{dl}} = \frac{\partial\sigma}{\partial\psi_{\text{dl}}} = -\text{sgn}(\psi_{\text{dl}})\left(\frac{Z^2q^2\varepsilon_0\varepsilon c}{2kT}\right)^{1/2}\frac{e^{\beta qZ\psi_{\text{dl}}} - e^{-\beta q\psi_{\text{dl}}}}{\left(Ze^{-\beta q\psi_{\text{dl}}} + e^{\beta qZ\psi_{\text{dl}}} - 1 - Z\right)^{1/2}} \quad (6)$$

The advantage of the regulation parameter are its simple values for the classical boundary conditions of constant charge (CC, $p = 1$) and constant potential (CP, $p = 0$).

Once the solution of eq. (2) for a given separation *h* is known, corresponding pressure Π acting between the plates can be obtained from the relation[1,16,39]

$$\Pi = kTc\left(Ze^{-\beta q\psi_{\text{mp}}} + e^{\beta qZ\psi_{\text{mp}}} - 1 - Z\right) \quad (7)$$

where $\psi_{\text{mp}} = \psi(0)$ is the midplane potential. As direct force measurements are often carried out with by means of larger microparticles, the measured force can be calculated from the Derjaguin approximation[1,39]

$$\frac{F}{R_{\text{eff}}} = 2\pi\int_h^\infty \Pi(h')\,dh' \quad (8)$$

where R_{eff} is the effective radius. The reason why we consider the normalized force F / R_{eff} is that this quantity is proportional to the surface energy. In the symmetric sphere-sphere geometry, which will be used here, the effective radius is given by $R_{\text{eff}} = R/2$ where *R* is the radius of the microparticles.

The relevant situation for the present system occurs when the multivalent ions are highly charged ($Z \gg 1$) and when their charge has the same sign as the surface charge. Thereby, the multivalent ions are excluded from the vicinity of the surface, which leads to a formation of a salt-free layer containing monovalent couterions only. Only rather far away from the interface, the presence of multivalent ions induces regular screening. Within the salt-free layer, the PB equation can be solved analytically, and one finds[28]

$$\Pi = \frac{\pi}{2} \cdot \frac{kT}{(h + 2L_{\mathrm{GC}})^2 L_{\mathrm{B}}} - kT(1 + Z)c \tag{9}$$

where L_{GC} is the Gouy-Chapman length

$$L_{\mathrm{GC}} = \frac{2\varepsilon_0 \varepsilon kT}{q|\sigma|} \tag{10}$$

and L_{B} is the Bjerrum length

$$L_{\mathrm{B}} = \frac{q^2}{4\pi\varepsilon_0 \varepsilon kT} \simeq 0.71 \text{ nm} \tag{11}$$

The numerical value of the Bjerrum length refers to water at room temperature. The double-layer layer thickness h_{dl} can be estimated from eq. (9) invoking the condition

$$\Pi(h_{\mathrm{dl}}) = 0 \tag{12}$$

When the electrolyte is strongly asymmetric and the multivalent ions have the same sign of charge as the interface, the PB model predicts an unusual non-exponential dependence of the respective pressures and forces. Typical results are shown in Fig. 1. In the linear representation shown in Fig. 1a,b one observes that starting at a well-defined distance the profiles decay very rapidly in the strongly asymmetric electrolyte, and that the interactions are basically negligible beyond that distance. This behavior is more clearly seen in the semi-logarithmic representation in Fig. 1c,d and it becomes increasingly pronounced with the increasing asymmetry of the electrolyte. The reason for this behavior is that the highly charged co-ions are excluded from the vicinity of the interface, and the interactions are dominated by a salt-free layer over a wide range of distances. The presence of the co-ions becomes only important at larger distances, and in this region the regular, strong screening sets in. Figure 1c further illustrates effects of boundary conditions. For the strongly asymmetric electrolyte, these conditions only affect the forces at very short separations. Already at intermediate distances, the forces are determined by the decay in the salt-free layer and they become independent of the boundary conditions. The behavior suggested by eq. (9) is also shown in that subfigure, and for a highly asymmetric electrolyte one observes that this relation is able to predict the pressure profile at intermediate distances very well. The double-layer layer thickness h_{dl} obtained from eq. (12) is also indicated in Fig. 1a,c.

Experimental

Materials. Aqueous suspensions of silica and latex nanoparticles were used. The silica nanoparticle suspension labeled as HS40 was purchased from Sigma-Aldrich, while the polystyrene sulfate latex nanoparticles from Invitrogen. The particle size distribution was obtained with transmission electron microscopy (TEM, Tecnai G2, FEI). The particle concentration was determined by weight from suspensions dried overnight at 110°C, and these values were in good agreement with the values reported by the manufacturer. The respective nanoparticle properties are summarized in Table 1. The mean particle radius and polydispersity of the latex nanoparticles determined by us are in good agreement with the values given by the manufacturer. The manufacturer of the latex further reports a nanoparticle charge of –440, which is expressed in units of the elementary charge per particle, as measured by conductometric titrations. Further details concerning the characterization of the same silica nanoparticle batch are given elsewhere.[20]

Silica nanoparticle suspensions were purified by ultrafiltration against pure water (Milli-Q, Millipore) with membranes with a molecular mass cut-off of 5000 g/mol (Amicon, Millipore) for about one week. Latex nanoparticle suspensions were dialyzed against pure water with membranes with a cut-off of 500 g/mol, also for about a week. In both cases, the filtrate conductivity dropped below 20 µS/cm. The pH of the dialyzed suspensions was measured with a standard glass electrode, and we found about 9.5 for silica and about 4.0 for latex. This difference could be caused by traces of disolved carbon dioxide or salts due to incomplete exchange of ions. We report nanoparticle concentrations as number concentrations in molar units. The nanoparticle number concentration *c* was obtained from their volume fraction ϕ from the relation $\phi = 4\pi a^3 c / 3$ where *a* is the mean particle radius determined by TEM. The volume fraction was calculated from the weight fraction by assuming ideal mixing. Polydispersity effects are neglected throughout.

Nanoparticle suspensions were further characterized by dynamic and electrophoretic light scattering (Zetasizer Nano ZS, Malvern). Dynamic light scattering was carried out in 1.0 mM NaCl solutions at particle concentrations of 5.0 g/L, which corresponds to particle concentrations of 3.2 µM for silica and 1.4 µM for the latex. The correlation functions were analyzed with second cumulant method and they yield the hydrodynamic radii given in Table 1. Comparison with the TEM values indicates that the extent of aggregation in these suspensions is minor. Electrophoretic mobility measurements were carried out in NaCl solutions within the concentration range of 1–20 mM for the silica nanoparticles at pH 9.5 and a particle concentration of 3.0 g/L (1.9 µM), while for the latex at pH 4.0 and a particle concentration of 1.0 g/L (0.28 µM) . The electrokinetic potential (ζ-potential) was obtained with the method of O'Brien and White.[1,41] These measurements confirmed that both types of nanoparticles are negatively charged.

Direct force measurements. Colloidal probe technique was used to measure forces with a closed-loop AFM (MFP-3D, Asylum Research, USA) placed on an optical microscope (Olympus IX 73). We use silica microparticles (Bangs Laboratories Inc., USA) with a radius of about 2.5 μm as colloidal probes. These microparticles were glued to tip less cantilevers (HQ CSC37, MikroMasch, Tallin, Estonia) and they were also sprinkled on a flat quartz substrate. Such cantilevers and substrates were sintered during 3 hours at 1150°C. The sintering leads to a firm attachment of the microparticles and removes the remaining glue. Thereby, the surface roughness of the microparticles is reduced and their radius shrinks to about 2.2 μm.[42]

Force measurements are carried out in the symmetric sphere-sphere geometry. The substrates and cantilevers are first treated in an air-plasma for 20 min and then mounted in the AFM-fluid cell. A pair of particles is centered with the optical microscope. Subsequently, approach and retraction cycles are measured at a velocity of 0.5 μm/s. The cantilever response is corrected by subtracting the baseline and the constant compliance region. A trigger point of 2 V was used to assure that the microparticles were in contact, and the optical lever sensitivity was fitted in the region of 0.60–0.95 V. Occasional particle adhesion events resulted in a poor constant compliance region, and these traces were excluded from further data analysis. The force is then obtained with the spring constant, which typically was in the range 0.2–0.5 N/m. The latter value is estimated from the thermal frequency response of the cantilever and its lateral dimensions with the method described by Sader et al.[43] Force profiles were obtained by averaging of about 100 approach and retraction cycles, leading to a force resolution of about 2 pN and a distance resolution below 0.5 nm. The resulting forces were further block averaged, and normalized to the effective radius R_{eff} .

The sphere-sphere geometry was also used to verify the diffuse layer potential of the microparticles in 1.0 mM NaCl solutions at pH 4.0 and 9.5. The force profile was interpreted within the PB model in monovalent electrolytes.[1,44] Least-squares fits yield diffuse layer potentials of –43±5 mV for pH 4.0 and –73±14 mV for pH 9.5. These values are in good agreement with previous measurements for similar silica microparticles.[44]

Results and discussion

Here, we present direct force measurements between a pair of similar silica microparticles in aqueous suspensions of two types of nanoparticles with the AFM. The microparticles have a radius of about 2.2 μm, while the silica and polystyrene nanoparticles about 6 and 11 nm, respectively. The situation is schematically depicted in the graphical abstract. The surfaces of the microparticles as well as of the nanoparticles are negatively charged. The nanoparticle suspensions used are basically salt-free, and therefore their surface charge is neutralized by monovalent ions. Earlier force measurements in similar systems reveal the existence of oscillatory forces. The present work confirms the presence of such forces at larger separation distances. At shorter distances, however, the forces are soft and strongly repulsive. These repulsive forces originate from double layer overlap and they feature an unusual non-exponential dependence. As we shall demonstrate, however, this dependence is fully compatible with PB theory. Note PB theory is only applicable at shorter distances, and not the oscillatory region at larger distances.

Experimental force profiles. Typical results for measured force profiles in silica and latex nanoparticle suspensions are shown in Figs. 2 and 3, respectively. The two columns refer to two different particle concentrations. Both systems feature the same qualitative behavior.

At larger distances, one observes weak oscillatory forces persisting over several periods. The wavelength of these oscillations decreases with increasing particle concentrations, while their amplitude increases. We report the particle concentrations as molar number concentrations. For the silica nanoparticle suspensions shown in Fig. 2, the respective number concentrations of 32 µM and 126 µM correspond to volume fractions of 0.023 and 0.087, and to mass fractions of 0.050 and 0.18. For the latex suspensions shown in Fig. 3, the number concentrations of 6.0 µM and 14 µM correspond to volume fractions of 0.019 and 0.047, and the respective mass fractions are close to identical to the latter values. Thus, all suspensions studied are relatively concentrated. Similar oscillatory forces were reported in suspensions of various types of nanoparticles and by different techniques earlier.[6-13] These oscillatory forces are induced by the liquid-like structure of the nanoparticle suspensions.[1,16]

At shorter distances, however, the interaction forces become strongly repulsive. This repulsion typically sets in at distances of few tenths of nm, and it is much stronger than the oscillatory forces. This feature is poorly visible in the linear representation (Fig. 2a and 3a), but clearly in the semi-logarithmic one (Fig. 2b and 3b). This repulsive force increases over 2–3 orders of magnitudes beyond the amplitude of the oscillatory force before the microparticles get into contact. The contact point is reached for a normalized force of about 20 mN/m in the silica nanoparticle suspensions, while about 3 mN/m are sufficient in the latex suspension. The difference between these two values also suggests that the microparticles are more charged in the suspension of silica nanoparticles than for the latex. One further observes that force profiles are virtually identical upon approach and retraction. This concurrence confirms the conservative nature of these forces. As will be argued below, this repulsive force is caused by the overlap of electrical double layers.

Qualitatively similar pressure profiles were found between charged walls in asymmetric electrolytes containing multivalent co-ions with integral equation theories.[34] This study also reports oscillatory forces at larger distances and monotonic, strongly repulsive forces at smaller distances. However, the comparison cannot be made quantitative, since the valence of the co-ions was rather small, and in contrast to the present study, substantial concentrations of monovalent salt were considered. Analogous results were also reported for suspensions charged nanoparticles interacting with screened Coulomb potential in slit geometries[36], but that study reports concentration profiles only.

Forces profiles were measured at various nanoparticle concentrations, and they were quantified by means of two different models. At large distances, these forces were represented with a damped oscillatory function, while at smaller distances the PB model was used. The comparison between the experimental and calculated force profiles in these two regimes will be discussed in the following.

Quantifying the large-distance behavior. At larger distances, the oscillatory forces can be well modeled with an exponentially decaying trigonometric function[12,28]

$$\frac{F}{R_{\text{eff}}} = Ae^{-h/\xi} \cos\left(\frac{2\pi h}{\lambda} + \theta\right) \tag{13}$$

where A is the amplitude, the ξ correlation (or decay) length, the λ wavelength, and θ the phase shift. This type of oscillatory profiles were suggested earlier for hard-sphere and charged sphere systems on theoretical grounds.[18,45-48] As shown in Fig. 2, this function is indeed capable to describe the force profile at larger distances very well. At smaller distances, however, the depth of the first minimum in the force profile is overestimated, which indicates an additional repulsive force, as already remarked earlier.[29] At very small distances, however, eq. (13) underestimates the actual force dramatically. Nevertheless, when the fitting is restricted to larger distances, one can extract all the parameters entering eq. (13). We have observed that the correlation length ξ shows no clear trend with particle concentration. Their values scatter around a mean of 25±5 nm in the silica suspensions, and 28±4 nm in the latex suspensions, whereby the error bar represents the standard deviation. For this reason we have fixed this parameter to the respective mean values, and refitted the force curves. The quality of the fits remains almost the same. In this fashion, we are able to reliably extract the concentration dependence of the wavelength λ, of the amplitude A, and of the phase shift θ.

Figure 4a shows the fitted wavelength λ versus the particle concentration c together with the power-law dependence suggested by eq. (1). The latter appears as a straight line in the double logarithmic plot used, and represents the measured values rather well. However, the values in the silica nanoparticle suspensions are typically located above the line, while the ones for the latex below. Moreover, the scatter of the data points involving the latex nanoparticle suspension is larger than for the silica nanoparticles. This scatter is probably caused by the smaller magnitude of the forces in the latex nanoparticle system. Note that we have already reported a subset of the present wavelength measurements in the same silica nanoparticle suspensions earlier.[20]

Similar oscillatory forces were already reported for various types of aqueous nanoparticle suspensions with interferometry[6,7], optical tweezers[8], or colloidal probe AFM.[9-13] The respective wavelengths are given in Fig. 4b and more details on these systems in Table 2. One observes that wavelengths reported in the literature follow precisely the same dependence on the particle concentration as found in the present work.

Figure 5 shows the other two fitted parameters entering the oscillatory profile given by eq. (13). These are the amplitude A, which is shown in Fig. 5a, and the phase shift θ, which is shown in Fig. 5b. One observes that both parameters increase with increasing particle concentration. The scatter of the data points for the latex nanoparticle suspensions is again larger than for silica, probably for the same reason as mentioned above.

Quantifying the small-distance behavior. As evident in the semi-logarithmic representations of the force profiles shown in Figs. 2 and 3, the damped oscillatory profile fails to describe the profiles at shorter distances. The force becomes strongly repulsive, and this force is caused by the overlap of the double layers. This part of the force profile can be well described with PB theory, but the nanoparticle suspension must be modeled as a strongly asymmetric electrolyte. Thereby, the nanoparticles represent the multivalent co-ions, while the counter ions are monovalent. When the PB model is extended to this situation, one can quantify the force profiles at small distances very well, see Figs. 2 and 3.

These fits involve four parameters, namely the diffuse layer potential of the silica probe microparticle $\psi_{\rm dl}$, the corresponding regulation parameter p, the number concentration c of the nanoparticles and their valence $Z_{\rm eff}$. The latter parameter will be referred to as the effective valence (or the magnitude of the effective charge) to stress that this charge is different from the bare charge of the nanoparticles.

The number concentration c of the nanoparticles is known from the suspension preparation, and thus can be fixed to the appropriate value. Least-squares fitting of the short-range part of the force profiles for the remaining parameters, we find that the regulation parameter decreases with particle concentration somewhat, but the scatter of the resulting values is substantial. One finds similar values for silica and latex nanoparticle suspensions, and the overall average yields p = 0.68±0.15, whereby the error bar is the standard deviation. In the present case of the highly asymmetric electrolyte, charge regulation effects are only important at very short distances, and therefore the actual value of this parameter affects the calculated double layer forces only marginally (see Fig. 1c). We have therefore fixed the regulation parameter to the mean value, and refitted all force profiles. Typical best fits are shown in Figs. 2 and 3.

The fact that the PB theory yields and excellent description of the data at shorter distances might seem surprising, especially given the assumption of point-like ions. At these distances, however, the multivalent co-ions are expelled from the slit, and the electrolyte in between is dominated by the monovalent counter ions only. Such a system can be naturally described with the PB model well. Note that the PB theory becomes invalid at larger distances, especially where oscillatory forces occur. The PB theory is based on a mean-field approach, which neglects all correlations. In the oscillatory region, however, strong correlations between the nanoparticles are present.

With these constraints, two parameters can be determined form the force profiles, namely the diffuse layer potential $\psi_{\rm dl}$ of the probe microparticles and the valence $Z_{\rm eff}$ of the nanoparticles. The values of the fitted parameters are summarized in Fig. 6.

Figure 6a shows the diffuse layer potential of the microparticles versus the particle concentration. One observes that this potential increases with increasing concentration. The magnitude of the diffuse layer potential is substantially lower in the latex nanoparticle suspensions than in the silica suspensions. This difference in charging is probably due to the different pH values of the two suspensions. The observed concentration dependence can be captured reasonably well with the charge-potential relationship given in eq. (4). Thereby, we have used a surface charge density of the microparticles in the silica and latex suspensions of –28 mC/m^2 and –6 mC/m^2, respectively. These values also suggest that the microparticles are more weakly charged in the latex particle suspensions than in the silica suspensions.

The fitted magnitude of the effective charge is shown in Fig. 6b. This parameter shows no clear dependence with nanoparticle concentration, and can be best represented with a constant. This fact further supports the validity of the PB model of the asymmetric electrolyte. The respective averages for the silica and latex nanoparticles are 88±6 and 230±30, whereby the error bars represent the standard deviation. These values are also summarized in Table 3. These numbers can also be expressed as surface charge densities, and one finds –26 mC/m^2 for silica nanoparticles and –24 mC/m^2 for the latex. Note that the former value is close to the value for the silica microparticles under same conditions.

Electrophoresis experiments represent another way to determine the effective charge. However, these experiments cannot be carried out in the concentrated nanoparticle suspensions used for the force measurements, and lower particle concentrations must be used. To adjust the concentration of the monovalent counter ions, we use the range of the concentration of the monovalent counter ions in the nanoparticle suspensions around 1–20 mM. This estimate follows from the effective charges reported above and the particle concentrations used. We have thus measured the electrophoretic mobility of the silica and latex nanoparticles suspended in solutions with NaCl concentrations in the range of 1–20 mM adjusted to pH 9.5 and 4.0, respectively. The measured electrokinetic potentials were then converted to surface charge densities with the extension of the Grahame equation for spheres valid for intermediate salt levels.[1] For silica and latex nanoparticles, one finds –19±4 mC/m^2 and –29±8 mC/m^2, respectively. These values then lead to the following magnitudes of the effective nanoparticle charge of 65 and 280, respectively. These estimates agree reasonably well with the effective charges extracted from the force measurements, see Table 3.

In salt-free conditions, the effective charge of highly charged nanoparticles can be further estimated from PB theory by means of the relation[49,50]

$$Z_{\mathrm{eff}} = \frac{6a}{L_{\mathrm{B}}} \tag{14}$$

where a is the radius of the nanoparticle, and L_{B} is the Bjerrum length given by eq. (11). Taking the measured mean radii from TEM, this relation suggests magnitudes of the effective charges for the silica and latex nanoparticles of 55 and 90, respectively. Table 3 indicates that these estimates are of the right order of magnitude, but they underestimate the measured effective charges by about a factor of two. The reason for these discrepancies could be caused by neglecting polydispersity effects, the finite size of the nanoparticles in the PB description, or remaining traces of salt.

The distinction between an effective and a bare charge is relevant.[51-54] An effective charge controls the strength of mutual interactions between the nanoparticles in a suspension, and enters the screened Coulomb potential. A bare charge corresponds to the actual number of charged groups on the particle surface. For a highly charged nanoparticle, the effective charge is normally much smaller than the bare charge, and is independent of the bare charge of the particle due to a saturation effect.[50,52,53]

For the presently investigated nanoparticles, the fact that the magnitude of the bare charge is much larger than the one of the effective charge can be seen as follows. Potentiometric titrations of various silica suspensions indicate that at similar pH and lower salt concentrations, the surface charge density is around –100 mC/m^2.[55-57] For the presently investigated silica nanoparticles, this number leads to a magnitude of the bare charge of about 300. A similar observation can be made for the latex nanoparticles based on the reported magnitude of the bare charge of about 440. Both numbers are larger than any of the estimates given in Table 3. This observation suggests indeed that one extracts from the present force measurements the effective charge of these nanoparticles.

Thickness of the particle-free layer. An additional important finding of the present study is the presence of a nanoparticle-free layer close to the interface. The presence of this layer is marked by strong repulsive double layer forces, which can be well described by PB theory for an asymmetric electrolyte. The simplest way to estimate the thickness of this layer from the experimental force profiles is by locating the position of the first zero in the experimental force profile. Figure 7 shows these estimates versus the particle concentration. One observes that the thickness of this layer decreases with increasing particle concentration, as one would expect since the electrostatic screening increases as well. We have also plotted the calculated double layer thickness h_{dl} obtained from eq. (12), which corresponds to the thickness of the particle-free layer in the PB model. To perform this calculation, we assume a constant diffuse layer charge density σ, as reported in the caption of Fig. 6, and a constant effective valence Z_{eff}, as given in the second column in Table 3. Given the fact that these calculations contain no adjustable parameters, the agreement with the experimental values is excellent.

These observations concerning the particle-free layer are in line with previous studies.[19,20,58] The presence of a particle-free layer close to a negatively charged water-solid interface in suspensions of the same (or similar) silica nanoparticles was established by neutron and X-ray reflectivity[19,20], and in suspensions of much larger polystyrene latex nanoparticles with a radius of about 35 nm with a quartz crystal microbalance.[58] Two of these studies also report a decrease of the thickness of the particle-free layer with increasing particle concentration.

The existence of a particle-free layer is also in agreement with theoretical studies of charged particle suspensions interacting by means the screened Coulomb potentials next to like-charged walls.[37,59] These authors used integral equation theories and computer simulations to investigate isolated interfaces as well as slit geometries. In all situations investigated, the existence of particle-free layers was predicted. Strongly repulsive forces at small separation distances were also predicted to act between charged interfaces in asymmetric electrolytes, where the co-ions had the same charge as the interface.[34]

Predicting the phase shift. When the thickness of the particle-free layer is known, the phase shift θ entering the oscillatory force profile given by eq. (13) can be estimated from the condition[28]

$$\frac{2\pi h_{\mathrm{dl}}}{\lambda} + \theta = \frac{5\pi}{2} \tag{15}$$

whereby the wavelength λ is calculated from of eq. (1). The condition given in eq. (15) physically means that the structural force vanishes at the onset of the particle-free layer and that at that point the pressure is positive.

The solid lines shown in Figs. 5b represent the calculated phase shift. No adjustable parameters enter these calculations, and one observes that these predictions are in good agreement with experiment.

Conclusions

Direct force measurements by means of silica microparticles are carried out in suspensions of negatively charged nanoparticles. At larger separation distances, the interactions feature oscillatory force profiles. These structural forces originate from the liquid-like structure of the nanoparticle suspensions. At smaller distances, one observes soft and strongly repulsive forces, which lead to a particle-free layer close to the water-solid interface. These forces are caused by double layer repulsion between the like-charged surfaces. While these forces are strongly non-exponential, they can be quantitatively interpreted with the Poisson-Boltzmann (PB) model for asymmetric electrolytes. From this description, which is only valid at short distances, the effective charge of the nanoparticles can be extracted. This charge is well comparable to the one obtained from electrophoresis, and to the saturation charge estimated from PB theory.

Currently, we have no reliable model to describe the transition regime between the double layer repulsion at short distances to the structural force at larger distances. A simple superposition of these two forces represents a reasonable approximation only for the silica nanoparticle suspension, but fails for the latex. The reason for this difference is that the structural forces are much weaker than double-layer forces in the silica suspension, and therefore the latter mask the contribution of the oscillatory force at shorter distances. However, these two contributions are more comparable in the latex suspension, and the oscillatory force modifies the short range region in an unphysical fashion.

The quantitative description of the transition regime will require a more detailed treatment of the structuring of nanoparticle suspensions near a charged water-solid interface. Modeling the nanoparticle suspension with hard-spheres interacting with screened Coulomb potential appears as the most promising approach to pursue.

Acknowledgements

This research was supported by the Swiss National Science Foundation through the project no. 178759 and University of Geneva.

Table 1. Particle radii and densities of the nanoparticles used.

	Mean Radius		Polydispersity (CV)	Density[c]
	TEM[a]	DLS[b]	TEM[a]	(g/mL)
Silica	6.5±0.1	8.2±0.3	0.17±0.03	2.29±0.02
Latex	10.9±0.1	12.1±0.1	0.19±0.02	1.06±0.01

[a]Determined in dry state by transmission electron microscopy. [b]Hydrodynamic radius measured by DLS. [c]From Ref. [20] for silica and from the manufacturer for the latex.

Table 2. Measurements of oscillatory interaction profiles in nanoparticle suspensions from literature. The respective wavelengths are reported in Fig. 4b.

Nanoparticles	Radius (nm)	Interface	Reference
Silica	9.5	Glass[a]	Nikolov et al. (1992)[6]
Polystyrene-polybutadiene latex	87	Glass, air[a]	Basheva et al. (1997)[7]
Polystyrene latex	42	Polymethacrylate[b]	Crocker et al. (1999)[8]
Polystyrene latex	11, 16	Silica[c]	Piech et al. (2002)[9]
Silica	11	Silica[c]	Piech et al. (2004)[10]
Silica	11	Silica[c]	Tulpar et al. (2006)[11]
Silica	5.5, 8.0, 13	Silica[c]	Zeng et al. (2011)[12]
Silica	5.1, 7.9, 13	Silica[c]	Ludwig et al. (2019)[13]

[a]Interferometry, [b]optical tweezers, [c]colloidal probe.

Table 3. Magnitude of the effective charge Z_{eff} of nanoparticles as obtained by different methods.

	Force measurement	Electrophoresis	Saturation PB model
Silica	88±6	70±10	55
Latex	230±30	280±80	90

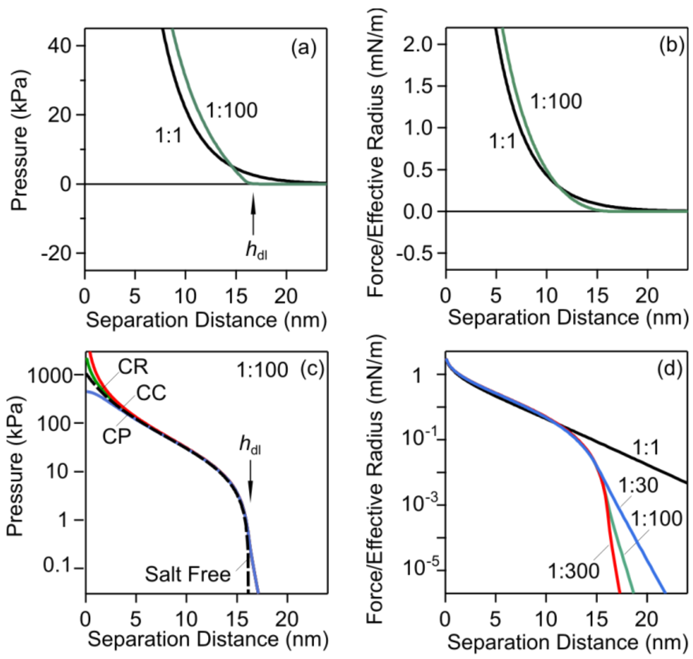

Figure 1. Interactions between negatively charged plates in solutions of 1:*Z* electrolytes versus the separation distance calculated with PB theory in (a,b) linear and (c,d) semi-logarithmic representation. (a,c) Pressure and (b,d) normalized force. The surface charge density is –25 mC/m^2 and the counter ion concentration 10 mM. Panel (c) indicates effects of boundary conditions with constant charge (CC), constant potential (CP), and constant regulation (CR) with regulation parameter p = 0.5. The dashed line is the pressure calculated with the approximate relation for the salt-free system given in eq. (9). Arrows indicate the double layer thickness h_{dl} .

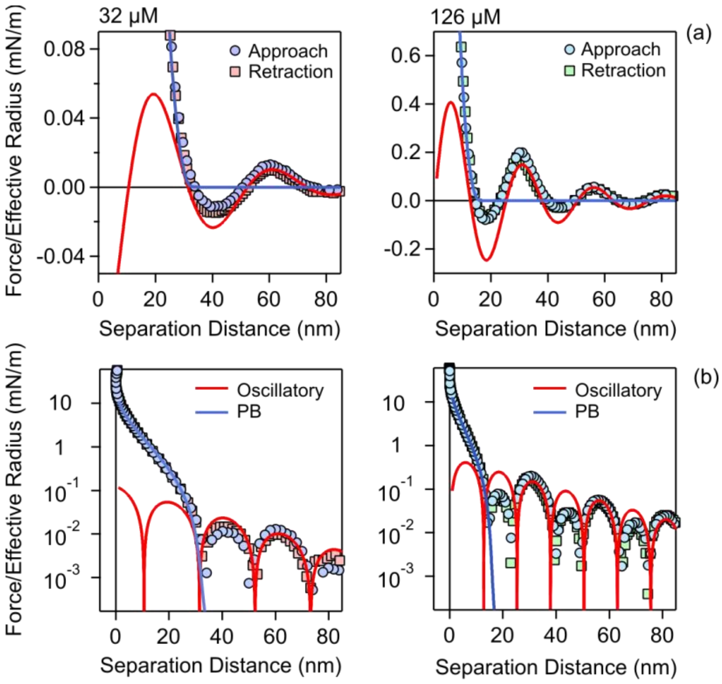

Figure 2. Normalized forces versus separation in silica nanoparticle suspensions in (a) linear and (b) semi-logarithmic representation of their magnitude. Experimental data upon approach and retraction are compared with calculations with PB theory and damped oscillatory profile given in eq. (13). Nanoparticle concentration of 32 μM is shown in the left column and 126 μM in the right one.

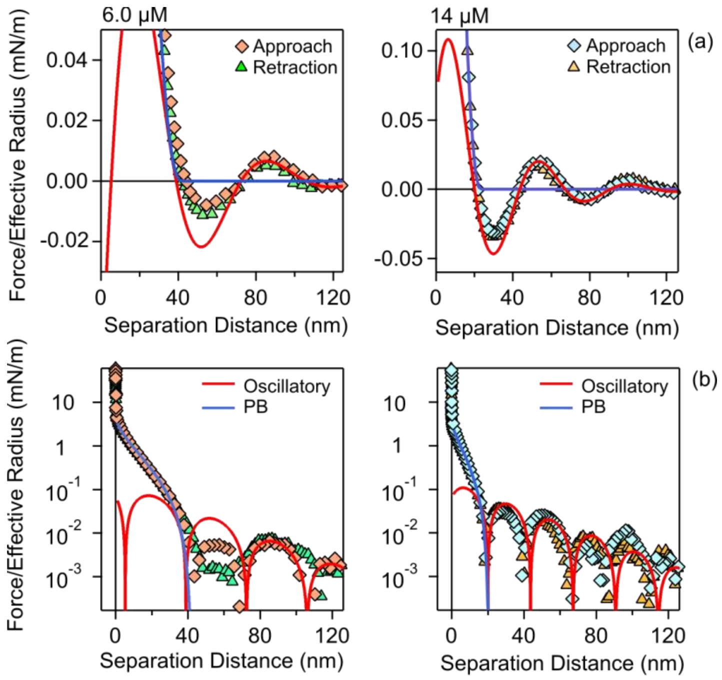

Figure 3. Normalized forces versus separation in polystyrene latex nanoparticle suspensions in (a) linear and (b) semi-logarithmic representation of their magnitude. Experimental data upon approach and retraction are compared with calculations with PB theory and damped oscillatory profile given in eq. (13). Nanoparticle concentration of 6.0 μM is shown in the left column and 14 μM in the right one.

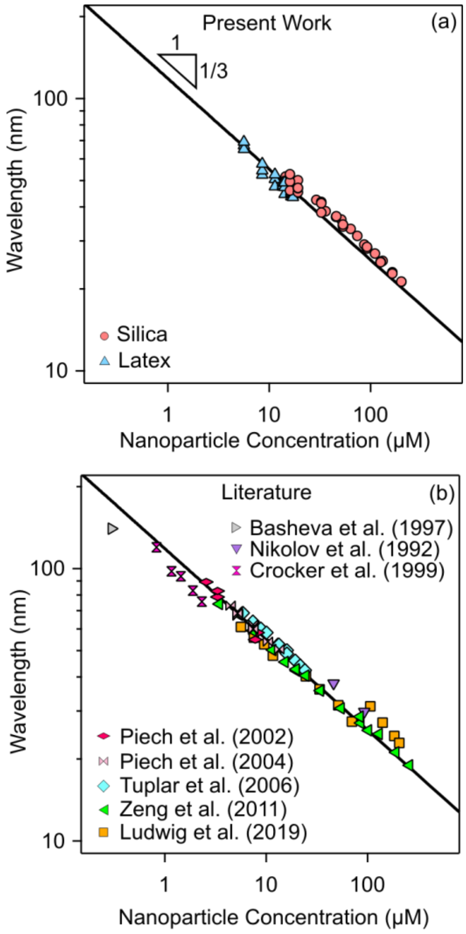

Figure 4. Wavelengths extracted from oscillatory force profiles versus nanoparticle concentration. Solid line is the scaling relation given in eq. (1). (a) Present work and (b) literature data. Further details on the literature data shown in (b) can be found in Table 2.

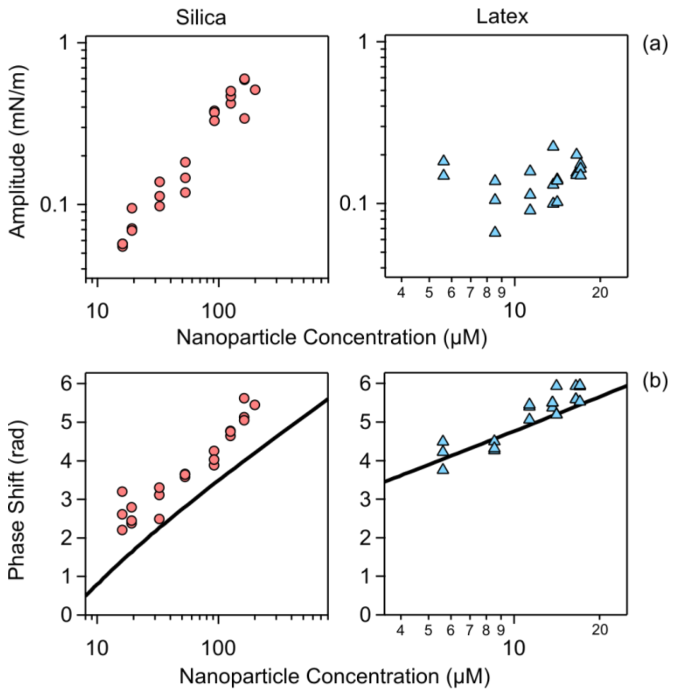

Figure 5. Parameters extracted from the oscillatory part of the measured force profiles versus the nanoparticle concentration. Data for silica and latex nanoparticle suspensions are shown in left and right columns, respectively. (a) Amplitude and (b) phase shift. The solid lines in (b) are predictions based on eq. (15).

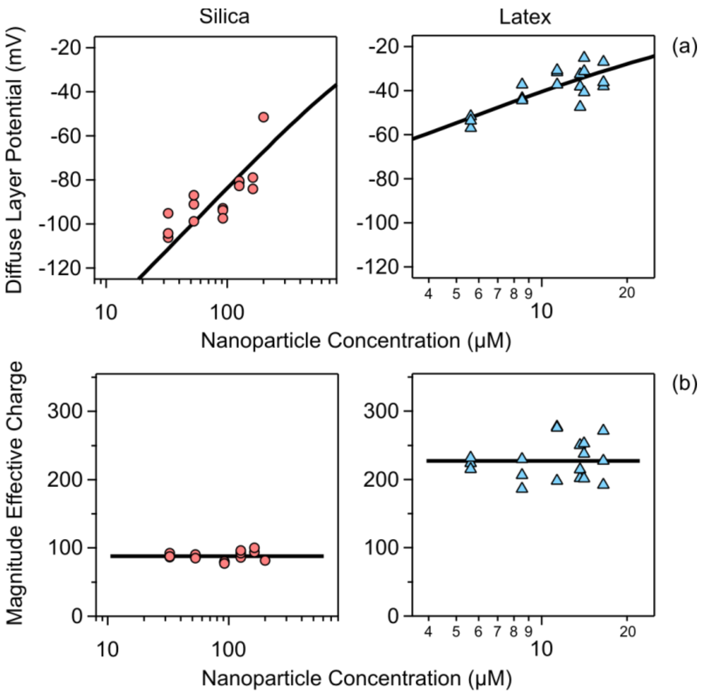

Figure 6. Parameters extracted from the measured force profiles with the PB model versus the nanoparticle concentration. Data for silica and latex nanoparticle suspensions are shown in left and right columns, respectively. (a) Amplitude and (b) phase shift. (a) Diffuse layer potential of the probe microparticle and (b) magnitude of the effective charge in units of the elementary charge of the nanoparticles in suspension. Solid lines in (a) are calculations with the PB model assuming a charge density of–28 mC/m^2 for silica and–6 mC/m^2 for the latex. Solid lines in (b) are constant values of the effective valence of 88 for silica and 230 for the latex.

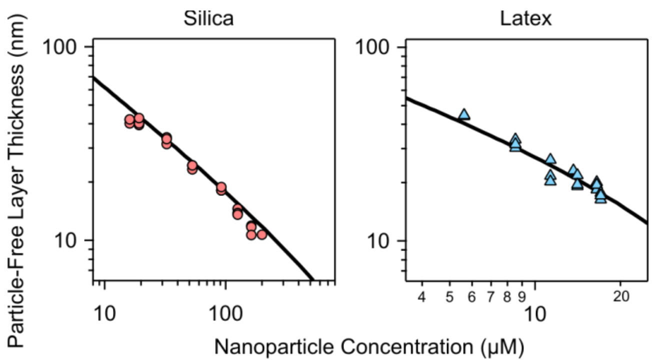

Figure 7. Thickness of the particle-free layer versus the nanoparticle concentration. Data for silica and latex nanoparticle suspensions are shown in the left and right subfigure, respectively. Solid lines are predictions based on eq. (12).

References

1. Russel, W. B.; Saville, D. A.; Schowalter, W. R., *Colloidal Dispersions*. Cambridge University Press: Cambridge, 1989.
2. Matijevic, E.; Babu, S. V., Colloid Aspects of Chemical-Mechanical Planarization. *J. Colloid Interface Sci.* **2008,** 320, 219-237.
3. Mezzenga, R.; Schurtenberger, P.; Burbidge, A.; Michel, M., Understanding Foods as Soft Materials. *Nature Mater.* **2005,** 4, 729-740.
4. Balzer, B.; Hruschka, M. K. M.; Gauckler, L. J., Coagulation Kinetics and Mechanical Behavior of Wet Alumina Green Bodies Produced via DCC. *J. Colloid Interface Sci.* **1999,** 216, 379-386.
5. Gesenhues, U., The Mechanism of Polyelectrolyte-Assisted Retention of TiO_2 Filler Particles during Paper Formation. *Adv. Colloid Interface Sci.* **2011,** 162, 1-21.
6. Nikolov, A. D.; Wasan, D. T., Dispersion Stability Due to Structural Contributions to the Particle Interaction as Probed by Thin Liquid-Film Dynamics. *Langmuir* **1992,** 8, 2985-2994.
7. Basheva, E. S.; Danov, K. D.; Kralchevsky, P. A., Experimental Study of Particle Structuring in Vertical Stratifying Films from Latex Suspensions. *Langmuir* **1997,** 13, 4342-4348.
8. Crocker, J. C.; Matteo, J. A.; Dinsmore, A. D.; Yodh, A. G., Entropic Attraction and Repulsion in Binary Colloids Probed with a Line Optical Tweezer. *Phys. Rev. Lett.* **1999,** 82, 4352-4355.
9. Piech, M.; Walz, J. Y., Direct Measurement of Depletion and Structural Forces in Polydisperse Charged Systems. *J. Colloid Interface Sci.* **2002,** 253, 117-129.
10. Piech, M.; Walz, J. Y., The Structuring of Nonadsorbed Nanoparticles and Polyelectrolyte Chains in the Gap Between a Colloidal Particle and Plate. *J. Phys. Chem. B* **2004,** 108, 9177-9188.
11. Tulpar, A.; Van Tassel, P. R.; Walz, J. Y., Structuring of Macroions Confined between Like-Charged Surfaces. *Langmuir* **2006,** 22, 2876-2883.
12. Zeng, Y.; Grandner, S.; Oliveira, C. L. P.; Thunemann, A. F.; Paris, O.; Pedersen, J. S.; Klapp, S. H. L.; von Klitzing, R., Effect of Particle Size and Debye Length on Order Parameters of Colloidal Silica Suspensions under Confinement. *Soft Matter* **2011,** 7, 10899-10909.
13. Ludwig, M.; Witt, M. U.; von Klitzing, R., Bridging the Gap between Two Different Scaling Laws for Structuring of Liquids under Geometrical Confinement. *Adv. Colloid Interface Sci.* **2019,** 269, 270-276.
14. Xing, X. C.; Hua, L.; Ngai, T., Depletion versus Stabilization Induced by Polymers and Nanoparticles: The State of the Art. *Curr. Opin. Colloid Interface Sci.* **2015,** 20, 54-59.
15. Butt, H. J.; Cappella, B.; Kappl, M., Force Measurements with the Atomic Force Microscope: Technique, Interpretation and Applications. *Surf. Sci. Rep.* **2005,** 59, 1-152.
16. Israelachvili, J., *Intermolecular and Surface Forces*. 3 ed.; Academic Press: London, 2011.
17. Smith, A. M.; Borkovec, M.; Trefalt, G., Forces between Solid Surfaces in Aqueous Electrolyte Solutions. *Adv. Colloid Interf. Sci.* **2020,** 275, 102078.

18. Klapp, S. H. L.; Zeng, Y.; Qu, D.; von Klitzing, R., Surviving Structure in Colloidal Suspensions Squeezed from 3D to 2D. *Phys. Rev. Lett.* **2008,** 100, 118303.
19. Nygard, K.; Konovalov, O., Decay of Interfacial Fluid Ordering Probed by X-Ray Reflectivity. *Soft Matter* **2012,** 8, 5180-5186.
20. Maroni, P.; Gvaramia, M.; Kosior, D.; Kubiak, K.; Scarratt, L.; Smith, A. M.; Merkel, D. G.; Bottyan, L.; Borkovec, M., Structuring of Colloidal Silica Nanoparticle Suspensions near Water-Silica interfaces probed by Specular Neutron Reflectivity. *Phys. Chem. Chem. Phys.* **2020,** 22, 6449-6456.
21. Milling, A. J., Depletion and Structuring of Sodium Poly(Styrene Sulfonate) at the Silica-Water Interface. *J. Phys. Chem.* **1996,** 100, 8986-93.
22. Milling, A. J.; Kendall, K., Depletion, Adsorption, and Structuring of Sodium Poly(Acrylate) at the Water-Silica Interface. 1. An Atomic Force Microscopy Force Study. *Langmuir* **2000,** 16, 5106-5115.
23. Uzum, C.; Christau, S.; von Klitzing, R., Structuring of Polyelectrolyte (NaPSS) Solutions in Bulk and under Confinement as a Function of Concentration and Molecular Weight. *Macromolecules* **2011,** 44, 7782-7791.
24. Biggs, S.; Dagastine, R. R.; Prieve, D. C., Oscillatory Packing and Depletion of Polyelectrolyte Molecules at an Oxide-Water Interface. *J. Phys. Chem. B* **2002,** 106, 11557-11564.
25. McNamee, C. E.; Tsujii, Y.; Ohshima, H.; Matsumoto, M., Interaction Forces between Two Hard Surfaces in Particle-Containing Aqueous Systems. *Langmuir* **2004,** 20, 1953-1962.
26. Christov, N. C.; Danov, K. D.; Zeng, Y.; Kralchevsky, P. A.; von Klitzing, R., Oscillatory Structural Forces due to Nonionic Surfactant Micelles: Data by Colloidal-Probe AFM vs Theory. *Langmuir* **2010,** 26, 915-923.
27. Theodoly, O.; Tan, J. S.; Ober, R.; Williams, C. E.; Bergeron, V., Oscillatory Forces from Polyelectrolyte Solutions Confined in Thin Liquid Films. *Langmuir* **2001,** 17, 4910-4918.
28. Moazzami-Gudarzi, M.; Kremer, T.; Valmacco, V.; Maroni, P.; Borkovec, M.; Trefalt, G., Interplay between Depletion and Double Layer Forces acting between Charged Particles in Solutions of Like-Charged Polyelectrolytes. *Phys. Rev. Lett.* **2016,** 117, 088001.
29. Schon, S.; von Klitzing, R., Experimental Evaluation of Additional Short Ranged Repulsion in Structural Oscillation Forces. *Soft Matter* **2018,** 14, 5383-5392.
30. Forsman, J., Surface Forces in Electrolytes Containing Polyions and Oppositely Charged Surfaces. *Curr. Opin. Colloid Interface Sci.* **2017,** 27, 57-62.
31. Gonzalez-Tovar, E.; Lozada-Cassou, M., Long-Range Forces and Charge Inversions in Model Charged Colloidal Dispersions at Finite Concentration. *Adv. Colloid Interface Sci.* **2019,** 270, 54-72.
32. Naji, A.; Kanduc, M.; Forsman, J.; Podgornik, R., Perspective: Coulomb Fluids - Weak Coupling, Strong Coupling, in Between and Beyond. *J. Chem. Phys.* **2013,** 139, 150901.

33. Levin, Y., Electrostatic Correlations: From Plasma to Biology. *Rep. Prog. Phys.* **2002,** 65, 1577-1632.
34. Jimenez-Angeles, F.; Odriozola, G.; Lozada-Cassou, M., Stability Mechanisms for Plate-Like Nanoparticles Immersed in a Macroion Dispersion. *J. Phys. Condes. Matter* **2009,** 21.
35. Jonsson, B.; Broukhno, A.; Forsman, J.; Akesson, T., Depletion and Structural Forces in Confined Polyelectrolyte Solutions. *Langmuir* **2003,** 19, 9914-9922.
36. Gonzalez-Mozuelos, P.; Alejandre, J.; Medina-Noyola, M., Structure of a Colloidal Suspension Confined in a Planar Slit. *J. Chem. Phys.* **1991,** 95, 8337-8345.
37. Gonzalez-Mozuelos, P.; Alejandre, J., Rogers-Young Approximation for the Concentration Profile of a Colloidal Suspension in Front of a Highly Repulsive Wall. *J. Chem. Phys.* **1996,** 105, 5949-5955.
38. Gonzalez-Mozuelos, P.; Medina-Noyola, M.; D'Aguanno, B.; Mendez-Alcaraz, J. M.; Klein, R., Concentration Profiles of a Colloidal Mixture Near a Charged Wall. *J. Chem. Phys.* **1991,** 95, 2006-2011.
39. Trefalt, G.; Szilagyi, I.; Borkovec, M., Poisson-Boltzmann Description of Interaction Forces and Aggregation Rates Involving Charged Colloidal Particles in Asymmetric Electrolytes. *J. Colloid Interf. Sci.* **2013,** 406, 111-120.
40. Trefalt, G.; Behrens, S. H.; Borkovec, M., Charge Regulation in the Electrical Double Layer: Ion Adsorption and Surface Interactions. *Langmuir* **2016,** 32, 380-400.
41. O'Brien, R. W.; White, L. R., Electrophoretic Mobility of a Spherical Colloidal Particle. *J. Chem. Soc. Farad. Trans. II* **1978,** 74, 1607-1626.
42. Valmacco, V.; Elzbieciak-Wodka, M.; Besnard, C.; Maroni, P.; Trefalt, G.; Borkovec, M., Dispersion Forces Acting Between Silica Particles across Water: Influence of Nanoscale Roughness. *Nanoscale Horizons* **2016,** 1, 325 - 330.
43. Sader, J. E.; Chon, J. W. M.; Mulvaney, P., Calibration of rectangular atomic force microscope cantilevers. *Rev. Sci. Instrum.* **1999,** 70, 3967-3969.
44. Smith, A. M.; Maroni, P.; Borkovec, M.; Trefalt, G., Measuring Inner Layer Capacitance with the Colloidal Probe Technique. *Colloids Interfaces* **2018,** 2, 65.
45. Evans, R.; de Carvalho, R. J. F. L.; Henderson, J. R.; Hoyle, D. C., Asymptotic Decay of Correlations in Liquids and their Mixtures. *J. Chem. Phys.* **1994,** 100, 591-603.
46. Trokhymchuk, A.; Henderson, D.; Nikolov, A.; Wasan, D. T., A Simple Calculation of Structural and Depletion Forces for Fluids/Suspensions Confined in a Film. *Langmuir* **2001,** 17, 4940-4947.
47. Grodon, C.; Dijkstra, M.; Evans, R.; Roth, R., Homogeneous and Inhomogeneous Hard-Sphere Mixtures: Manifestations of Structural Crossover. *Mol. Phys.* **2005,** 103, 3009-3023.
48. Adar, R. M.; Safran, S. A.; Diamant, H.; Andelman, D., Screening Length for Finite-Size Ions in Concentrated Electrolytes. *Phys. Rev. E* **2019,** 100, 042615.

49. Chew, W. C.; Sen, P. S., Potential of a Sphere in an Ionic Solution in Thin Double Layer Approximations. *J. Chem. Phys.* **1982,** 77, 2042-2044.
50. Aubouy, M.; Trizac, E.; Bocquet, L., Effective Charge Versus Bare Charge: An Analytical Estimate for Colloids in the Infinite Dilution Limit. *J. Phys. A* **2003,** 36, 5835-5840.
51. Wette, P.; Schope, H. J.; Palberg, T., Comparison of Colloidal Effective Charges from Different Experiments. *J. Chem. Phys.* **2002,** 116, 10981-10988.
52. Palberg, T.; Monch, W.; Bitzer, F.; Piazza, R.; Bellini, T., Freezing Transition for Colloids with Adjustable Charge: A Test of Charge Renormalization. *Phys. Rev. Lett.* **1995,** 74, 4555-4558.
53. Gisler, T.; Schulz, S. F.; Borkovec, M.; Sticher, H.; Schurtenberger, P.; D'Aguanno, B.; Klein, R., Understanding Colloidal Charge Renormalization from Surface Chemistry: Experiment and Theory. *J. Chem. Phys.* **1994,** 101, 9924-9936.
54. Trizac, E.; Bocquet, L.; Aubouy, M.; von Grunberg, H. H., Alexander's Prescription for Colloidal Charge Renormalization. *Langmuir* **2003,** 19, 4027-4033.
55. Hiemstra, T.; de Wit, J. C. M.; van Riemsdijk, W. H., Multisite Proton Adsorption Modeling at the Solid-Solution Interface of (Hydr)Oxides: A New Approach 2. Application to Various Important (Hydr)Oxides. *J. Colloid Interface Sci.* **1989,** 133, 105-117.
56. Dove, P. M.; Craven, C. M., Surface Charge Density on Silica in Alkali and Alkaline Earth Chloride Electrolyte Solutions. *Geochim. Cosmochim. Acta* **2005,** 69, 4963-4970.
57. Kobayashi, M.; Juillerat, F.; Galletto, P.; Bowen, P.; Borkovec, M., Aggregation and Charging of Colloidal Silica Particles: Effect of Particle Size. *Langmuir* **2005,** 21, 5761-5769.
58. Hellsing, M. S.; Rennie, A. R.; Rodal, M.; Hook, F., Charged Polystyrene Nanoparticles near a SiO_2/Water Interface. *Langmuir* **2019,** 35, 222-228.
59. Gonzalez-Mozuelos, P.; Alejandre, J.; Medina-Noyola, M., Electrostatic Adsorption of Colloidal Particles on the Walls of a Planar Slit: Simulation versus Theory. *J. Chem. Phys.* **1992,** 97, 8712-8721.

Table of Contents Graphic (TOC)